Int J Adv Manuf Technol (2018) 95:825–834
https://doi.org/10.1007/s00170-017-1261-6

ORIGINAL ARTICLE

Self-supporting interior structures modeling for buoyancy optimization of computational fabrication

Dawei Li[1] · **Ning Dai**[1] · **Xin Zhou**[1] · **Renkai Huang**[1] · **Wenhe Liao**[1]

Received: 27 May 2017 / Accepted: 24 October 2017 / Published online: 4 November 2017

Abstract Interior structures including lattice, porous, or cellular structures have been widely used in geometric design for 3D printing. It can not only reduce the weight of objects but also adjust the physical properties, such as stress, balance, and center of mass. In this work, we present a novel method for buoyant equilibrium and optimization of the material distribution inside an object, such that the 3D printed object satisfies prescribed constraints of mass properties. In particular, we introduce a mathematical method to describe the internal structure compactly, and prove that this compact formulation generates density-variable lattice structures to control the mass properties precisely. Additionally, this internal structure has shown itself to be capable of self-supporting in 3D printing processing. We demonstrate the effectiveness of our mathematically based method for generating interior patterns in the applications of optimizing shapes that stably float in liquids, and in improving mechanical stiffness.

Keywords Buoyancy optimization · Self-supporting structures · Physical modeling · 3D printing

1 Introduction

3D printing technologies significantly extend the geometric design space and liberate the designer's creativity, particularly through the research of the computational methods. They provide an easy and intuitive control over the physical properties of the printed object [1]. One of the recurrent research problems in this field is the design of balance and the optimization of physical properties of the fabricated objects. Moreover, the physics of flotation have gradually become a popularly studied topic in the context of 3D printing technology, leading to innovations such as the design of offshore platforms with complex underwater structures, or optimizing ships with better balance performance, or objects for entertainment such as floating toys. The orientation of the floating object is defined by the shape of the object, the mass distribution, and the fluid displacement. These factors must be optimized so that the object can be stably floating at the desired orientation and waterline position. Moreover, unlike traditional hull design [2, 3], we are presented with a particular shape and required to make it float without changing its external appearance.

However, it is difficult to design a buoyant object with numerous constraints by hand. In many cases, the optimized structures cannot be directly fabricated by a layer-based 3D printing method. Especially, if the shape has a relatively large overhang, it needs additional interior support which can make an optimized model lose its balance, and it is hard to remove the internal surface supporting structures. Therefore, in this paper, we propose a computational fabrication method to design and optimize buoyancy and improve the manufacturability through a computer program.

First, for the buoyancy balance problem, we adopt the voxel carving method [4, 5] to manipulate the internal mass distribution of a designed object, and combined with the Archimedes principle [6], a set of buoyancy geometric calculation criteria is established. The user only provides the mesh of a 3D object, desired waterline position and floating orientation, and the densities of the fabrication material and target fluid. Then, the mechanical parameters and mass density

✉ Ning Dai
dai_ning@nuaa.edu.cn

Dawei Li
davidlee@nuaa.edu.cn

[1] College of Mechanical and Electrical Engineering, Nanjing University of Aeronautics and Astronautics, Nanjing 210016, China

distribution of an object will be calculated by our method. Next, with the mass distribution, the interior structure of the object is easy to distribute. Second, to obtain a better overall mechanical stiffness property, we will optimize full internal filling on the basis of buoyancy optimization in this work, instead of hollowing part of the area. Third, to overcome the manufacturability problem in internal structure optimization, we present a mathematically based method for infill optimization that ensures the resultant structures are self-supporting. We have selected a structure that has a high geometrically controllable performance and has been widely proven to have self-supporting capacity [7, 8] as our internal design structure, from a set of many of the similar mathematical structures. Specifically, this mathematical expression method can obtain continuously controllable density changes in space. The special contributions of our work are as follows:

- We use a compact parameterization of the shape's interior by a mathematical expression, which significantly reduces the number of design variables in shape interior optimization.
- We take account of manufacturability by the mathematical method to generate self-supporting structures living in a manufacturability-ensured space represented by a gyroid-like lattice.
- We demonstrate the effectiveness of our buoyancy optimization approach.

2 Related works

Recently, more and more researchers have been devoting to geometric and physical modeling for 3D printing techniques. In this section, we have discussed the advantages and limitations of current approaches most closely related to our work.

Balancing optimization This class of problems usually involves static and rotational stability and optimization by controlling the internal mass distribution of the shape. Prévost et al. [4] proposed an approach to optimize the balance of a shape to make it stand in a given pose. Furthermore, Bächer et al. [5] extended the work and provided a new optimization of the mass distribution to make an object spinnable around a given axis. With the above approaches, the interior of the object is discretized into voxels, and some voxels are hollowed to redistribute the object's mass. Xie et al. [9] mainly referred to this method to generate internal voids which not only satisfy the static and rotational stability functions but are also support-free during 3D printing. In our work, we adopt a similar design idea, but the voxels are just mapped to the density distribution and will be replaced by our mathematically based lattice structures. Additionally, different from the volume-based methods, Musialski et al. [10] optimized an offset surface of the input mesh as the interior shape and presented a subspace method to accelerate the internal form and showed a subspace method to speed up the computation. Christiansen et al. [11] presented an automatic, optimization-based method for balancing objects, and the object is embedded in an adaptive tetrahedral mesh, and the balance is then improved by creating internal cavities and by rotating the model around its base. Complementary to these works, we focus on buoyancy equilibrium properties resulting from mass distribution.

Buoyancy optimization Buoyancy equilibrium is also a balancing optimization problem, which has become a hot topic in the field of computational fabrication recently. In 2016, Wang et al. [12] introduced a design and manufacturing pipeline for optimizing buoyant equilibrium and stability of complex 3D shapes and applied a similar voxel carving technique [4, 5] to control the mass distribution. For high-precision fabrication, they employed 3D printing method and introduced a method for stacking laser cut planar pieces to create 3D objects for larger-scale designs. Recently, Wu et al. [13] proposed an extension of ray representation to shape interior modeling, and proven this compact formulation greatly reduces the number of design variables compared to the general volumetric element-wise formulation, and demonstrated the effectiveness for optimizing shapes that stably float in liquids. In contrast, Prévost et al. [14] introduced the approach of placing movable masses inside a 3D shape to consider multiple centers of mass depending on the object's pose, including the standing, suspension, and immersion balancing problem. Summarizing the above buoyancy optimization approaches are mainly through hollowing out local internal space of the model.

Interior structure optimization The internal structure optimization of an object can be realized for different objectives of physical properties. Similar to 2D texture mapping, Chen [15] presented a 3D texture design method which maps a lattice into a design space to generate internal structures, and this system is based on a microstructure library. Inspired by the construction of truss structures, Wang et al. [16] optimized the mechanical stiffness of objects' fabrication by using a skin-frame structure to support the shape's interior. Lu et al. [17] introduced a honeycomb-cell structure by gradually carving out the interior of an object, but the hollowed cells are enclosed. That makes it difficult to remove the internal supporting materials. Zhang et al. [18] proposed an internal supporting structure based on medial axis tree, and the internal results are more complex for 3D printing. Li et al. [19] introduced the method of controlling the parameters of the microstructures which can vary spatially to produce graded

materials, and combined with cross-sectional stress analysis method [20] to reinforce an object.

Self-supporting structures Among the above approaches, the interior structure cannot be fabricated directly without support structures. Thus, many approaches have been developed to reduce the usage of the support structure to optimize material usage, fabrication time, and surface quality. It mainly consists of optimizing the printing orientation [21, 22], supporting shapes [23, 24], and even splitting the model [25, 26]. In contrast, the structure with self-supporting ability will be able to better solve the manufacturing problem of the internal fabric of the object. Whereas, self-supporting structures have been extensively studied in the field of architectural geometry [27–29], and only the shape of a surface is optimized in most of these approaches. In 3D printing field, Wu et al. [30] proposed a rhombic cell which is self-supporting. As a concurrent work, Xie et al. [9] proposed a similar support-free interior carving by the rhombic cell for 3D printing. While their focuses are mainly on optimizing the static and rotational stability, we demonstrate our method by optimizing the buoyant stability of 3D printed objects.

3 Preprocessing

Given an input object and desired orientation and waterline, we optimize the density distribution to satisfy these properties. First, to preserve the external shape of the object, a hollowed shell structure is generated from an input surface mesh. An implicit function $f(x)$ is fitted by using the vertices of the input mesh using multi-level partition of unity (MPU) implicit [31]. As shown in Fig. 1a, the continuous function $f(x)$ gives an approximated distance between the interpolated surface and x. Therefore, the inner surface is obtained by contouring the isosurface $f(x) = d$. The parameter d is the thickness of the shell. Here, let Ω_I be an internal region of the shell structure. In the region Ω_I, we define the structured domain represented by voxels for density optimization as shown in Fig. 1b. Each voxel has eight grid points, and the value of the implicit function $f(x)$ is assigned to each grid point. If all eight grid points of a voxel have negative values, the voxel is labeled as an inside voxel. Otherwise, it is labeled as an outside voxel. Finally, we construct an optimization problem and solve it to assign density values to each voxel (Fig. 1c).

Density constraint We assume that the object consists of a single material whose density is ρ_{material}. Therefore, we consider ρ_i as a relative density value that takes the following range:

$$\rho_{\min} \le \rho_i \le 1 \qquad i = 0, 1, \ldots, N-1 \tag{1}$$

In this representation, $\rho_i = 1$ corresponds to ρ_{material}, and $\rho_{\min}$ is the minimum constant value of relative density that satisfies $0 < \rho_{\min} < 1$. The choice of value $\rho_{\min}$ is discussed in the following sections.

4 Procedural function-based modeling for shape interior

Given a polygonal mesh representing the boundary of a solid, we construct the triple periodic minimal surface structures as composites of the object's interior, and these structures have proven to have superior mechanical properties [32, 33] and self-supporting ability [7, 8] in additive manufacturing. The presentation of this type of lattice structure, the associated geometric operators, and the properties are presented in this section.

4.1 Self-supporting interior structure modeling based on mathematical method

There are numerous kinds of lattice structures consisting of triple periodic minimal surface (TPMS) which have been widely used in the fields of biomimetic and 3D printing geometric design. Particularly fascinating are minimal surfaces that have a crystalline structure, in the sense of repeating themselves in three-dimensional space, i.e., being triply periodic. These minimal surfaces have three lattice vectors, and they are invariant under translation along three independent directions. The most common ones are Schoen gyroid, Schwarz primitive, diamond, and Neovius. All TPMS can be expressed as [34]:

$$F(x,y,z) = \sum_{hkl} |F(hkl)| \cdot \cos\left(\frac{2\pi}{L}(hx + ky + lz) - \alpha_{hkl}\right). \tag{2}$$

where $F(hkl)$ denotes the structure factor amplitude, reflecting the symmetry of the structure; α_{hkl} the phase angle; and L the cubic unit cell edge length. The set of allowed hkl values of the Fourier components of the structure and the Fourier series representation of the space group can be found in the *International tables of X-ray crystallography* [34].

The TPMS which have an infinitely connected triply periodic non-self-intersecting minimal surface with triple junctions and which contain no straight lines on the surface are believed to be suitable for additive manufacturing. These cellular structures such as Schwarz diamond and Schoen gyroid surfaces are continuously curved geometries and self-supporting and are deemed to be suitable for SLA/DLP technology. These periodic cellular structures could be considered a potential for lightweight and support structure applications.

Through the level set isosurface algorithm, we can easily control the volume fraction of these lattice structures.

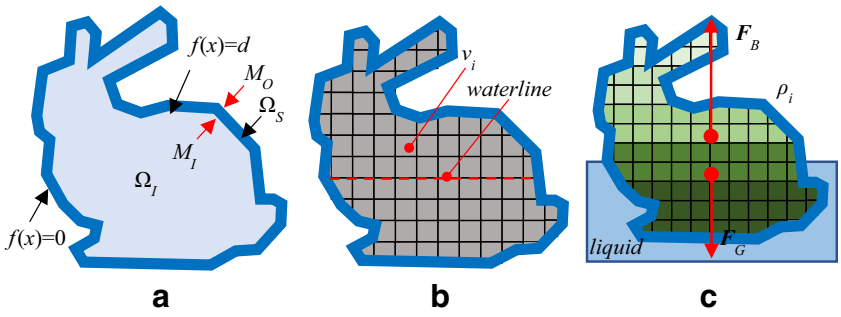

Fig. 1 **a** Generate the shell and internal region. **b** Inside voxels. **c** Density distribution meets the buoyancy

Moreover, the level surfaces are represented by function F: $\mathbb{R}^3 \rightarrow \mathbb{R}$ of points $(x, y, z) \in \mathbb{R}^3$, which satisfy the equation:

$$F(x, y, z) = t, \tag{3}$$

where t is a constant. The form of the surface is controlled by $F(x, y, z)$, while the parameter t determines the volume fraction of the areas that are separated by the surface. Figure 2 shows the relationship between the isosurface value and volume fraction for four typical TPMS functions. From this plot, we can find that only the Schoen gyroid structure appears to be linear at all volume fractions. Moreover, this linear property makes it easy to perform geometric control with volume fraction design. Thus, in this paper, we choose gyroid and gyroid-like lattice as our interior structure to control the density distribution of the floating bodies.

4.2 Density-variable modeling method and its properties

As the gyroid structure has superior and controllable geometric properties, in this work, we use this structure as the fill lattice. In this part, we will describe how to achieve continuous variable density design in detail. The level surface can approximate the single-gyroid of constant mean curvature:

$$F_{\mathrm{SG}}(x, y, z) = \sin\left(\frac{2\pi}{L}x\right)\cos\left(\frac{2\pi}{L}y\right) + \sin\left(\frac{2\pi}{L}y\right)\cos\left(\frac{2\pi}{L}z\right) + \sin\left(\frac{2\pi}{L}z\right)\cos\left(\frac{2\pi}{L}x\right) = t \tag{4}$$

At $t = 0$, Eq. (4) corresponds to the minimal gyroid surface. As the absolute value $|t|$ increases in the range between 0 and 1.413, the fraction of volume occupied by one of the regions decreases, whereas the complementary one increases. For $|t| > 1.413$, the surface becomes disconnected [19].

If we set parameter t to be a continuous function $t(\rho)$ in $\mathbb{R}^3$ with respect to the density value ρ, we will obtain a new structure in which the spatial density is continuously changed. Also, as long as the function $t(\rho)$ is a continuous function in the geometric space, it is possible to obtain a structure in which any continuous non-uniform density changes. As shown in Fig. 3a, we present a design case to illustrate the significance of variable density for buoyancy control design. The inverse function $\rho(t)$ of $t(\rho)$ is divided into two continuous segmented functions $\rho(t_1(x))$ and $\rho(t_2(x))$ in the x-direction, and they are continuous at point B. In this case, the $\rho(t_1(x))$ function's curvature rises rapidly when near the point B, so

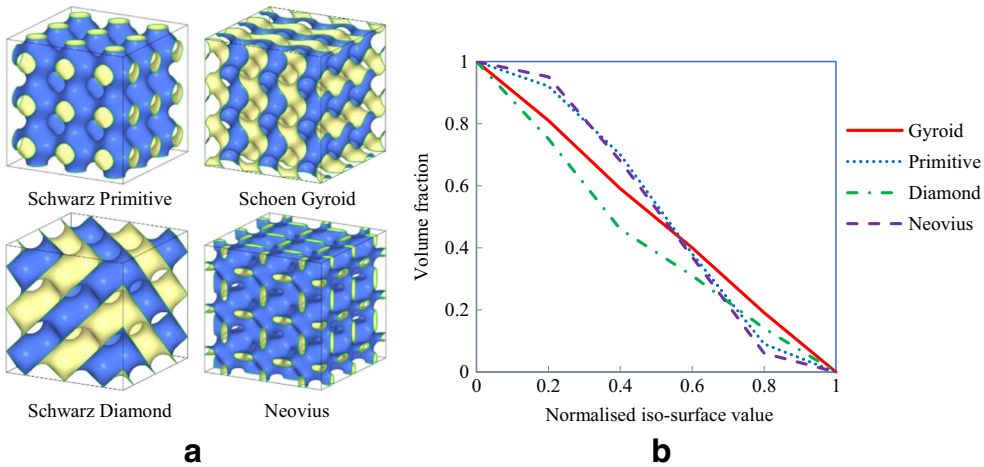

Fig. 2 **a** Four common implicit function geometric structures. **b** The relationship between isosurface value and volume fraction for selected implicit functions

that the structure can be quickly converted from the high-density value to low density, and then the function $\rho(t_2(x))$ is a low-density constant value function that takes $\rho(t_1(x))$ function's minimum, so that the BC segment is a low-density uniform change structure. Thus, not only can the overall mass center be controlled near the point A (the section AB accounts for 95% of overall mass), and the entire space can be filled to ensure a good overall stiffness. As shown in Fig. 3b, this gyroid-based density-variable structure is manufacturable by a 3D printing method and has a self-supporting ability.

4.3 Elastic modulus of gyroid structure

The mechanical properties of porous structures are often characterized by relatively Young's modulus, and it reflects the resistance-distortion ability of an object. Additionally, Young's modulus can be altered by variations in pore shape as well as pore distribution. According to [35]'s research, at low densities, experimental results indicate that Young's modulus of the porous structure is related to their density through the relation:

$$\frac{E}{E_s} = C\left(\frac{\rho}{\rho_s}\right)^n = C\overline{\rho}^n, \tag{5}$$

where E_s and ρ_s are Young's modulus and density of the solid material, and $\overline{\rho}$ is the relative density. Furthermore, Choren et al. [36] presented detail relationships between Young's modulus and volume porosity for additive manufacturing applications. Using similar expression, Khaderi et al. [37] calculated the stiffness and strength of gyroid structure and given the C as 0.465 and n as 2. Thus, it shows that each density value corresponds to a certain modulus, which can be used to design the minimum strength of an object. Then, the designer needs to give a certain infilling density value as the minimum density constraint $\rho_{\min}$, and this work is pure to verify our buoyancy optimization method. In this paper, according to gyroid's geometric properties [19], the minimum density constraint value is set as 0.05 that the gyroid has a minimal good complete continuous geometry structure.

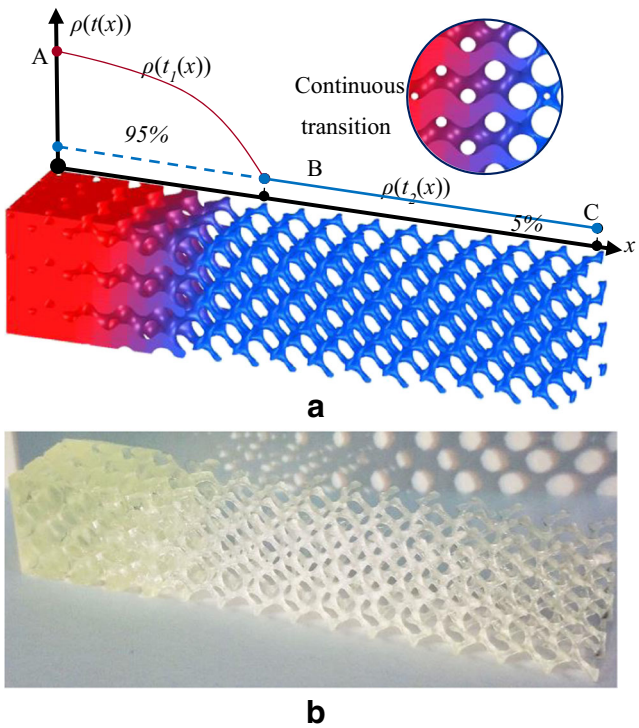

Fig. 3 **a** Gyroid-based density-variable structure generated and **b** self-supporting ability by 3D printing method

5 Optimizing buoyancy properties

The buoyancy, orientation, and stability of a floating object are closely related to the mass distribution of the object. In this paper, the above spatial density-variable controlled method is used to realize a stable equilibrium of a floating body when placed in the fluid. Equilibrium and stability are the two most important parameters in buoyancy optimization, whose equilibrium ensures that the object is in its designed orientation and waterline, and stability is the ability to restore balance when it is disturbed.

5.1 Equilibrium

According to Archimedes' principle, an unrestrained object is subject to two forces when in the liquid, its weight $\boldsymbol{F}_G$ and the buoyancy force $\boldsymbol{F}_B$, due to pressure acting on its surface. If the total force $\boldsymbol{F} = \boldsymbol{F}_G + \boldsymbol{F}_B$ does not vanish, an unrestrained body will accelerate in the direction $\boldsymbol{F}$ according to Newton's second law. Therefore, in mechanical equilibrium, gravity force and buoyancy must cancel each other precisely at all times to guarantee that the object will remain in place. Although an object may be in buoyant equilibrium, such that the total force composed of gravity and buoyancy vanishes, it may still not be in complete mechanical equilibrium. The total moment of all the forces acting on the body must also vanish; otherwise, an unrestrained body will necessarily start to rotate. The total moment is also a sum of two terms, $\boldsymbol{M} = \boldsymbol{M}_G + \boldsymbol{M}_B$, with one contribution from gravity, $\boldsymbol{M}_G = \boldsymbol{F}_G \times \boldsymbol{C}_G$, and the other from pressure called the moment of buoyancy, $\boldsymbol{M}_B = \boldsymbol{F}_B \times \boldsymbol{C}_B$, where $\boldsymbol{C}_G$ and $\boldsymbol{C}_B$ are the center of gravity and buoyancy of the object. If the total force is zero, the total moment will be independent of the origin of the coordinate system, as may be easily shown. In summary, the equilibrium equation of the floating body is as follows:

$$\begin{cases} \boldsymbol{F} = \boldsymbol{F}_G + \boldsymbol{F}_B = 0 \\ \boldsymbol{M} = \boldsymbol{M}_G + \boldsymbol{M}_B = 0 \end{cases} \tag{6}$$

And we assume the direction of gravity to be $\boldsymbol{g} = (0, 0, -\|\boldsymbol{g}\|)$.

5.2 Static stability

Stability is of great importance to a floating object. As shown in Fig. 4a, given a small disturbance displacement, the object may return to its original position (stable), or move away from its initial position (unstable). Stability depends on the relevant lines of action of forces on an object. The upward buoyancy force on an object acts through the center of buoyancy $\boldsymbol{C}_{\mathrm{B}}$, being the centroid of the displaced volume of fluid. The weight force on the object acts through its center of gravity $\boldsymbol{C}_{\mathrm{G}}$. A floating object will be stable if the center of gravity is beneath the center of buoyancy because any angular displacement will then produce a "restoring moment," The stability of a buoyant object at the surface is more complex, and it may remain stable even if the center of gravity is above the center of buoyancy, provided that when disturbed from the equilibrium position, the center of buoyancy moves further to the same side that the center of gravity moves, thus providing a positive restoring moment. If this occurs, the floating object is said to have a positive metacentric height, z_{MG} (as shown in Fig. 4b). This situation is typically valid for a range of heel angles, beyond which the center of buoyancy does not move enough to provide a positive restoring moment, and the object becomes unstable.

In equilibrium, the horizontal positions of the centers of buoyancy and gravity must be equal $x_{\mathrm{B}} = x_{\mathrm{G}}$ and $y_{\mathrm{B}} = y_{\mathrm{G}}$. The vertical position z_{B} of the center of buoyancy will normally be different from the vertical position of the center of gravity z_{G}, which depends on the actual mass distribution of the object, determined by its structure and load. In addition, when an object heels, the center of buoyancy of the object moves laterally. It might also move up or down concerning the water line. As shown in Fig. 4b left, the point M at which a vertical line through the heeled center of buoyancy crosses the line through the original; vertical center of buoyancy is the metacenter. The metacenter M remains directly above the center of buoyancy by definition, such that $x_{\mathrm{M}} = x_{\mathrm{B}} = x_{\mathrm{G}}$ and $y_{\mathrm{M}} = y_{\mathrm{B}} = y_{\mathrm{G}}$. Moreover, there is a relationship between the height of the metacenter z_{M} and vertical position z_{B} of the center of buoyancy [6]:

$$z_{\mathrm{M}} = z_{\mathrm{B}} + \frac{I}{V}. \tag{7}$$

where V is the volume of displaced fluid, I is the smallest second moment of the waterline area. The metacenter is a purely geometric quantity, depending only on the displacement volume V, the center of buoyancy z_{B}, and the second-order moment of the shape of the object in the waterline. When giving a small tilt angle α, it will generate a restoring moment $\boldsymbol{M}_{\mathrm{R}}$ around the x-axis to achieve stability, and in terms of the height of the metacenter z_{M}, the restoring moment is defined as:

$$\boldsymbol{M}_{\mathrm{R}} = \alpha(z_{\mathrm{G}} - z_{\mathrm{M}}) \times \boldsymbol{F}_{\mathrm{G}}. \tag{8}$$

For the buoyant object to be stable, the restoring moment must counteract the tilt and thus have opposite sign of the tilt angle α. Consequently, the stability condition becomes:

$$z_{\mathrm{G}} < z_{\mathrm{M}}. \tag{9}$$

Evidently, the floating body is only stable when the center of gravity lies below the metacenter. Morever, the larger the metacentric height, the larger the restoring moment and the harder the object is to overturn. Also, for a given designed waterline, the term I/V and z_B in (7) will be a constant value, and thus, z_{M} is a certain value. In this work, we aim to control z_{G} without changing the external shape. Additionally, it is also a special state of buoyancy balance when the object is submerged in a liquid. Because I is equal to zero in this condition, so the metacenter coincides with the center of buoyancy, and the constraint is still meet $z_{\mathrm{G}} < z_{\mathrm{M}}$.

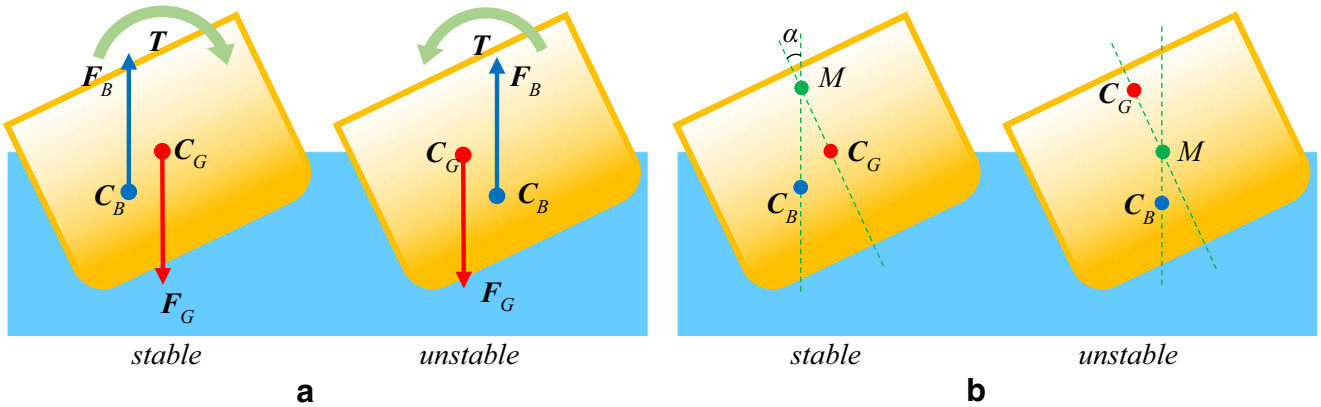

Fig. 4 **a**, **b** Given a small disturbance displacement, the object may return to its original position (stable), or move away from its original position (unstable)

5.3 Optimization implementation

The static status of floating of an object is related to its center of mass. The object floats if its buoyancy balances the gravity, and to maximize floating stability, its center of mass should be at its lowest possible position. For simplicity, we choose a coordinate frame such that the z-axis coincides with the intended perpendicular direction. Similar to [12, 13], the design problem is formulated as follows:

$$\begin{aligned} &\underset{v_i}{\text{minimize}} \quad z_G \\ &\text{s.t.}: \quad \boldsymbol{F}_G + \boldsymbol{F}_B = 0 \\ &\qquad x_M = x_B = x_G, y_M = y_B = y_G \\ &\qquad z_G < z_M \\ &\qquad v_{\min} \le v_i \le 1 \end{aligned} \tag{10}$$

We then can obtain the target center of gravity of the object, z_{G}^{*}, and it will be added as the center of mass constraint so that the target center of mass $\boldsymbol{C}_{\mathrm{G}}^{*} = \left(x_{\mathrm{G}}, y_{\mathrm{G}}, z_{\mathrm{G}}^{*}\right)$ is equal to the center of mass of the object (shell and density distribution).

$$\boldsymbol{C}_{\mathrm{G}}^{*} = \frac{\rho_{material}(V_{shell}\boldsymbol{c}_{shell} + \sum \rho_i v_i \boldsymbol{w}_i)}{\rho_{material}(V_{shell} + \sum \rho_i v_i)} \tag{11}$$

V_{shell} and $\boldsymbol{c}_{\mathrm{shell}}$ denote the volume and the center of mass of the shell structure, respectively, and $\boldsymbol{w}_i$ denotes the center of mass of the ith voxel. In addition, given the shape of the waterline area, the force of buoyancy $\boldsymbol{F}_{\mathrm{B}}$ is equal and opposite to the weight of the displaced fluid and the gravity force $\boldsymbol{F}_{\mathrm{G}}$, and thus, the gravity force $\boldsymbol{F}_{\mathrm{G}}$ is a constant value with a defined waterline. Therefore, we add a mass constraint so that the total target mass m^{*} is equal to the total mass of the object (shell and density distribution).

$$m^{*} = \rho_{material}(V_{shell} + \sum \rho_i v_i) \tag{12}$$

To assign a density value to satisfy the given mass properties, we should set an objective function with respect to the density value ρ_i of the ith voxel as expressed by Eq. (13). We use the Laplacian of mass to get a smooth density distribution usage similar to [38].

$$E = \sum_i \sum_{j \in N_i} \left(\rho_i v_i - \rho_j v_j\right)^2 \tag{13}$$

N_i and v_i denote a set of adjacent voxels of the ith voxel and the volume of the ith voxel, respectively. According to Eqs. (11)–(13), the above objective function can be converted to the following matrix form:

$$\begin{cases} \text{minimize} & \frac{1}{2}\boldsymbol{\rho}^{\mathrm{T}}\boldsymbol{Q}\boldsymbol{\rho} + \boldsymbol{c}^{\mathrm{T}}\boldsymbol{\rho} \\ \text{s.t.} & \boldsymbol{A}\boldsymbol{\rho} = \boldsymbol{b}, \qquad \boldsymbol{\rho}_{\min} \le \boldsymbol{\rho} \le 1 \end{cases} \tag{14}$$

The objective function described in Eq. (14) is a quadratic form, and the constraints are linear equality and inequality. Therefore, these equations can be interpreted as a linear constrained convex problem. We solve the problem using the interior point method [39]. We use the EIGEN matrix library as a quadratic programming solver to compute density for all inside voxels. An overview is illustrated in Fig. 5.

6 Results

Our proposed approach has been used for the optimization of several models with different geometric complexities, and we verified their behavior by placing them in a tank filled with pure water.

6.1 3D printing results

To demonstrate the effect of the buoyancy optimization and the manufacturability of the optimized shapes, we have fabricated some models using *Envisiontec-Micro-Edu* equipment with a transparent photopolymer. The density of the polymer printing material is 1.18–1.19 g/cm^3. As shown in Fig. 6, it is a

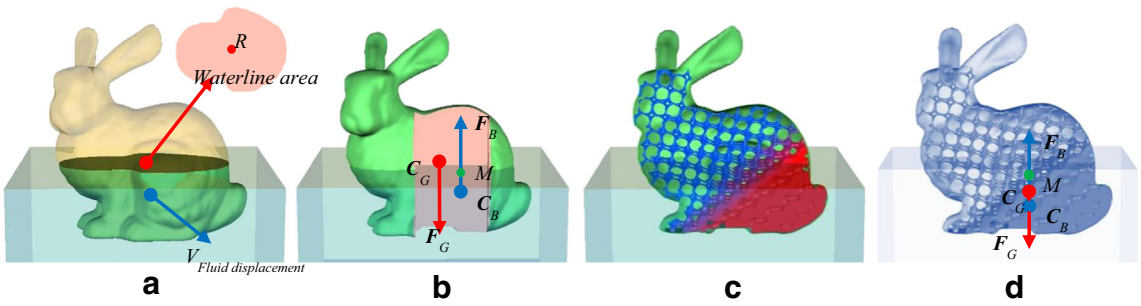

Fig. 5 Buoyancy optimization overview: **a** User input, solid model placed in the fluid. The fluid displacement, waterline area, and center of the roll are calculated for optimization. **b** Initially, the center of gravity and center of buoyancy are not vertically aligned. Additionally, the gravity force and the buoyancy force are typically not equal magnitudes. **c** A minimal thickness boundary shell is fixed. The interior space is voxelized and then hollowed. **d** Result, center of gravity and center of buoyancy align vertically and center of gravity lies below the metacenter (M)

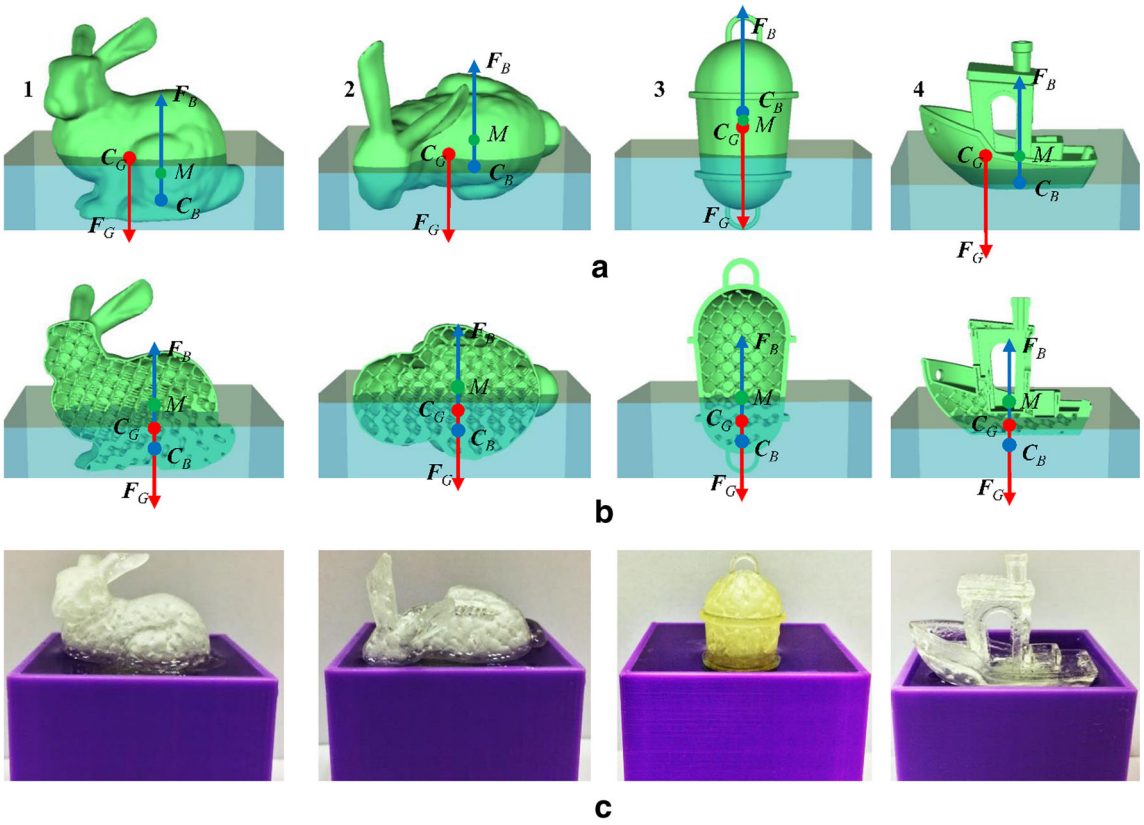

Fig. 6 Shapes optimized for stable floating: **a** On the upper of each group, the original object does not satisfy the floating stability criteria. **b** The middle one shows the optimized internal shape where the center of mass and the center of buoyancy are vertically aligned, and the center of mass is located in its lowest position, **c** The bottom image of each group shows the printed object stably floating in a water tank

set of models optimized for floating in water; 1 and 2 are the Stamford bunny in differently designed directions, 3 is an oceanic floater, and 4 is a boat. After optimization, the centers of mass of these objects are aligned vertically with the center of buoyancy, and the magnitude of the buoyant force and the magnitude of the gravity force are same. We then put these 3D printed floating bodies in a tank filled with pure water, and their orientations and positions in the liquid almost achieve the desired results of design. During the experiment, we measured the emersed height of the model in the direction of the z-axis, and the total experimental deviation could be controlled within 2 mm.

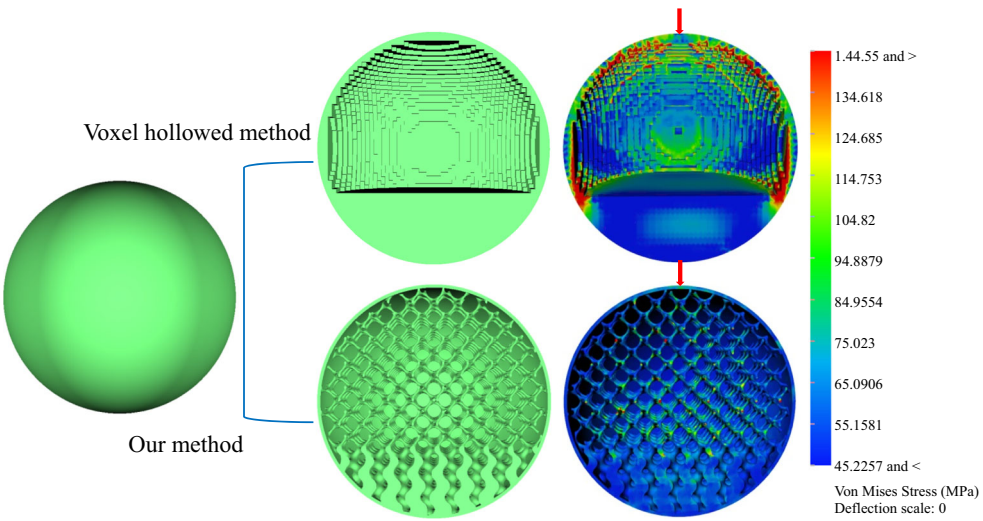

Fig. 7 Compared voxel hollowed method with ours under the same force conditions

6.2 Mechanical stiffness and self-supporting

To achieve the optimal solution, the most existing center of gravity optimization solutions is not considering the overall mechanical stiffness of the model, which is affected by hollowing out the object partially [4, 5, 12, 13]. In this work, the model's internal space is entirely filled with the lattice structures at the expense of a small amount of weight without affecting the optimization results of the model's balance, and which can give the object better overall mechanical stiffness. As shown in Fig. 7, we compared the voxel hollowing method with ours. It is evident that the model with a fulfilled internal lattice structure has better mechanical strength under the same force conditions.

Secondly, to allow removal of supporting material from the hollowed space, these models had to be printed in multiple segments and glued together afterwards, because the internal structure of these approaches created models without self-supporting capacity. In this way, not only is the operation too expensive, but also the support removal could cause overall quality deviations of the object and lead to inaccurate buoyancy optimization results. In this work, the self-supporting structure is used to fill the whole model, and it allows the complex inner surface of the model to be produced by 3D printing (As shown in Fig. 3).

7 Conclusion

We propose a novel method to control the mass properties of 3D printed objects for buoyancy optimization. In contrast to other approaches, our method not only optimizes the buoyancy balance but also considers the global stiffness of the model and the manufacturability of the internal structure. The proposed method consists of two steps. First, density distribution is optimized to satisfy mass properties which are calculated by given waterline and orientation condition. Second, an internal self-supporting structure is generated to represent the density distribution through mathematical expression. Finally, we have demonstrated the effectiveness of our buoyancy stability with numerous printed results and have shown the overall structural strength to be better than the local hollowing method. As future work, we will extend this approach to the design of other 3D printed objects' physical properties, such as rotation, stress distribution, and other relevant engineering applications.

Acknowledgements We would like to thank the anonymous reviewers for their constructive comments.

Funding information This work was supported by the National Science Foundation of China (Grant No. 51775273); Natural Science Foundation of Jiangsu Province, China (No. BK20161487); Six Talent Peaks Project in Jiangsu Province, China (No. GDZB-034); Aeronautical Science Foundation of China (No. 2015162024); Postgraduate Research and Practice Innovation Program of Jiangsu Province (Grant No. KYKX16_0320).

References

1. Umetani N, Bickel B, Matusik W (2015) Computational tools for 3D printing. SIGGRAPH Courses 9 p 1
2. Nowacki H (2010) Five decades of computer-aided ship design. Comput Aided Des 42(11):956–969
3. Biran A, Pulido RL (2013) Ship hydrostatics and stability. Butterworth-Heinemann
4. Prévost R, Whiting E, Lefebvre S, Sorkine HO (2013) Make it stand: balancing shapes for 3D fabrication. ACM Trans Graph (TOG) 32(4):81
5. Bächer M, Whiting E, Bickel B, Sorkine HO (2014) Spin-it: optimizing moment of inertia for spinnable objects. ACM Trans Graph (TOG) 33(4):96
6. Lautrup B (2011) Physics of continuous matter: exotic and everyday phenomena in the macroscopic world. CRC press, Boca Raton
7. Strano G, Hao L, Everson RM, Evans KE (2013) A new approach to the design and optimisation of support structures in additive manufacturing. Int J Adv Manuf Technol 66(9–12):1247–1254
8. Aremu AO, Maskery IA, Tuck CJ, Ashcroft IA, Wildman RD, Hague RJM (2016) Effects of net and solid skins on self-supporting lattice structures. Challenges Mech Time Depend Mater 2:83–89
9. Xie Y, Chen X (2017) Support-free interior carving for 3D printing. Vis Inform 1(1):9–15
10. Musialski P, Auzinger T, Birsak M, Ashcroft IA, Wildman RD, Hague RJM (2015) Reduced-order shape optimization using offset surfaces. ACM Trans Graph 34(4):102
11. Christiansen AN, Schmidt R, Bærentzen JA (2015) Automatic balancing of 3D models. Comput Aided Des 58:236–241
12. Wang L, Whiting E (2016) Buoyancy optimization for computational fabrication. Comput Graph Forum 35(2):49–58
13. Wu J, Kramer L, Westermann R (2016) Shape interior modeling and mass property optimization using ray-reps. Comput Graph 58: 66–72
14. Prévost R, Bächer M, Jarosz W, Jarosz W, Sorkinehornung O (2016) Balancing 3D models with movable masses. Proceedings of the Vision, Modeling and Visualization Workshop, vol 7
15. Chen Y (2007) 3D texture mapping for rapid manufacturing. Comput Aided Des Appl 4(6):761–771
16. Wang W, Wang TY, Yang Z, Liu L, Tong X, Tong W, Deng J, Chen F, Liu X (2013) Cost-effective printing of 3D objects with skin-frame structures. ACM Trans Graph (TOG) 32(6):177
17. Lu L, Shaft A, Zhao H, Wei Y, Fan QN, Chen X, Savoye Y, Tu CH, Daniel CO, Chen BQ (2014) Build-to-last: strength to weight 3D printed objects. ACM Trans Graph (TOG) 33(4):97
18. Zhang X, Xia Y, Wang J, Yang Z, Tu C, Wang W (2015) Medial axis tree—an internal supporting structure for 3D printing. Comput Aided Geom Des 35:149–162
19. Li D, Dai N, Jiang X, Jiang X, Chen X (2016) Interior structural optimization based on the density-variable shape modeling of 3D printed objects. Int J Adv Manuf Technol 83(9–12):1627–1635
20. Umetani N, Schmidt R (2013) Cross-sectional structural analysis for 3D printing optimization. SIGGRAPH Asia Technical Briefs 5: 1–5:4
21. Zhang X, Le X, Panotopoulou A, Whiting E, Wang CC (2015) Perceptual models of preference in 3D printing direction. ACM Trans Graph (TOG) 34(6):215
22. Ezair B, Massarwi F, Elber G (2015) Orientation analysis of 3D objects toward minimal support volume in 3D-printing. Comput Graph 51:117–124

23. Vanek J, Galicia JAG, Benes B (2014) Clever support: efficient support structure generation for digital fabrication. Comput Graph Forum 33(5):117–125
24. Dumas J, Hergel J, Lefebvre S (2014) Bridging the gap: automated steady scaffoldings for 3D printing. ACM Trans Graph (TOG) 33(4):98
25. Chen X, Zhang H, Lin J, Hu R, Lu L, Huang QX, Chen B (2015) Dapper: decompose-and-pack for 3D printing. ACM Trans Graph 34(6):213
26. Song P, Deng B, Wang Z, Dong Z, Li W, Fu CW, Liu L (2016) CofiFab: coarse-to-fine fabrication of large 3D objects. ACM Trans Graph (TOG) 35(4):45
27. Vouga E, Höbinger M, Wallner J, Pottmann H (2012) Design of self-supporting surfaces. ACM Trans Graph (TOG) 31(4):87
28. Deuss M, Panozzo D, Whiting E, Liu Y, Block P, Sorkinehornung O, Pauly M (2014) Assembling self-supporting structures. ACM Trans Graph (TOG) 33(6):214
29. Miki M, Igarashi T, Block P (2015) Parametric self-supporting surfaces via direct computation of airy stress functions. ACM Trans Graph (TOG) 34(4):89
30. Wu J, Wang CC, Zhang X, Westermann R (2016) Self-supporting rhombic infill structures for additive manufacturing. Comput Aided Des 80:32–42
31. Ohtake Y, Belyaev A, Alexa M, Turk G, Seidel HP (2005) Multi-level partition of unity implicits. ACM Siggraph 2005 Courses p 173
32. Abueidda DW, Dalaq AS, Al-Rub RKA, Younes HA (2015) Finite element predictions of effective multifunctional properties of interpenetrating phase composites with novel triply periodic solid shell architectured reinforcements. Int J Mech Sci 92:80–89
33. Lee W, Kang DY, Song J, Moon JH, Kim D (2016) Controlled unusual stiffness of mechanical metamaterials. Sci Rep 6
34. Scherer MRJ (2013) Gyroid and Gyroid-Like Surfaces. Double-Gyroid-Structured Functional Materials, pp 7–19
35. Roberts AP, Garboczi EJ (2001) Elastic moduli of model random three-dimensional closed-cell cellular solids. Acta Mater 49(2):189–197
36. Choren JA, Heinrich SM, Silver-Thorn MB (2013) Young's modulus and volume porosity relationships for additive manufacturing applications. J Mater Sci 48(15):5103–5112
37. Khaderi SN, Deshpande VS, Fleck NA (2014) The stiffness and strength of the gyroid lattice. Int J Solids Struct 51(23):3866–3877
38. Yamanaka D, Suzuki H, Ohtake Y (2014) Density aware shape modeling to control mass properties of 3D printed objects. ACM SIGGRAPH Asia 2014 Technical Briefs p 7
39. Bonnans JF, Gilbert JC, Lemaréchal C, Sagastizábal CA (2013) Numerical optimization: theoretical and practical aspects. Springer Science & Business Media